TISSUE ENGINEERING: Part A
Volume 19, Numbers 3 and 4, 2013

DOI: 10.1089/ten.tea.2012.0042

NELL-1 Injection Maintains Long-Bone Quantity and Quality in an Ovariectomy-Induced Osteoporotic Senile Rat Model

Jinny Kwak, DDS,[1,*] Janette N. Zara, MD,[2,3,*] Michael Chiang, BDS,[2] Richard Ngo, BS,[2] Jia Shen, PhD,[4] Aaron W. James, MD,[1] Khoi M. Le,[2] Crystal Moon,[2] Xinli Zhang, MD, PhD,[2] Zhongru Gou, PhD,[5] Kang Ting, DMD, DMedSci,[1,2,†] and Chia Soo, MD[4,†]

Over 10 million Americans have osteoporosis, and is the predominant cause of fractures in the elderly. Treatment of fractures in the setting of osteoporosis is complicated by a suboptimal bone regenerative response due to a decline in the number of osteoblasts, their function, and survival. Consequently, an osteogenic therapeutic to prevent and treat fractures in patients with osteoporosis is needed. Nel-like molecule-1 (NELL-1), a novel osteoinductive growth factor, has been shown to promote bone regeneration. In this study, we aim to demonstrate the capacity of recombinant NELL-1 to prevent ovariectomy (OVX)-induced osteoporosis in a senile rat model. Ten-month-old female Sprague-Dawley rats underwent either sham surgery or OVX. Subsequently, 50 μL of 600 μg/mL NELL-1 lyophilized onto a 0–50-μm tricalcium phosphate (TCP) carrier was injected into the femoral bone marrow cavity while phosphate-buffered saline (PBS) control was injected into the contralateral femur. Our microcomputed tomography results showed that OVX + PBS/TCP control femurs showed a continuous decrease in the bone volume (BV) and bone mineral density (BMD) from 2 to 8 weeks post-OVX. In contrast, OVX + NELL-1/TCP femurs showed resistance to OVX-induced bone resorption showing BV and BMD levels similar to that of SHAM femurs at 8 weeks post-OVX. Histology showed increased endosteal-woven bone, as well as decreased adipocytes in the bone marrow of NELL-1-treated femurs compared to control. NELL-1-treated femurs also showed increased immunostaining for bone differentiation markers osteopontin and osteocalcin. These findings were validated *in vitro*, in which addition of NELL-1 in OVX bone marrow stem cells resulted in increased osteogenic differentiation. Thus, NELL-1 effectively enhances *in situ* osteogenesis in the bone marrow, making it potentially useful in the prevention and treatment of osteoporotic fractures.

Introduction

Although frequently unrecognized until fractures occur, osteoporosis is the predominant cause of bone fractures in the elderly. It is estimated that more than 10 million Americans have osteoporosis; one in two Caucasian women and one in five men are expected to experience an osteoporosis-related fracture in the course of a lifetime.[1] Treatment and prevention of such fractures are complicated by suboptimal bone regenerative response due to osteoporosis. With the aging global population, the healthcare cost of treating osteoporosis-related fractures is expected to double or triple within the next four decades.[2,3] Consequently, there is an increasing need for improved osteogenic therapeutics to treat and/or prevent bone fractures in patients with osteoporosis.

Osteoporosis is a condition characterized by decreased bone mass and microarchitectural deterioration of bone tissue.[4,5] It is generally divided into two types—rapid loss of bone mass in postmenopausal osteoporosis due to estrogen deficiency, or the more gradual-onset senile osteoporosis seen in men and women that occurs with aging.[6] The underlying biologic conditions in patients with osteoporosis may include not only an increase in bone resorption due to changes in the microenvironment as in postmenopausal women, but also a decline in bone marrow stem cell (BMSC) content as seen with aging.[7] In addition, because osteoblasts and adipocytes are derived from the same BMSCs, age-related increased adipogenesis in the bone marrow leads to decreased osteoblastogenesis.[8] Therefore, there is a decrease in the number of osteoblasts, and findings have also shown a decrease in their function and survival.[5] For these reasons,

[1]Section of Orthodontics School of Dentistry, [2]Dental and Craniofacial Research Institute, [3]Department of Bioengineering, and [4]Department of Orthopaedic Surgery, University of California, Los Angeles, Los Angeles, California.
[5]Zhejiang-California International NanoSystems Institute, Zhejiang University, Hangzhou, China.
*Co-first authors.
†Co-senior authors.

the biologic responses to even the commonly used bone substitutes are suboptimal in such patients, in terms of efficacy and efficiency of bone regeneration and the frequency and magnitude of unwanted side effects.[9]

In terms of prevention therapy, parathyroid hormone (PTH) is the sole anabolic therapeutic approved by the Food and Drug Administration (FDA) for osteoporosis treatment, and has been shown to increase the BMSC population postirradiation. PTH, however, is anabolic only when given intermittently, and its use over 2 years has been shown to cause an increase in the development of bone neoplasms in rats.[10] Thus, PTH is limited to only once in a lifetime use and only for a limited duration to temporarily reverse osteopenia, soon after which the osteopenic/osteoporotic condition returns.[11] A commonly used antiresorptive agent, bisphosphonate, inhibits osteoclast activity in patients with osteoporosis to prevent further bone loss. However, systemic administration of bisphosphonate is associated with adverse effects, including bowel inflammation and erosion of the esophagus when taken orally; possible osteonecrosis of the jaw after high-dose intravenous administration in patients with cancer; severe bone, joint, or musculoskeletal pain; and fluctuation in calcium blood levels that may increase risk of cardiovascular events.[12] In addition, bisphosphonate is an anticatabolic agent only, and is not capable of regenerating bone. Therefore, an improved, alternative agent that would help prevent osteoporosis-related fractures without exhibiting unwanted systemic effects would be of tremendous clinical advantage.

Bone morphogenetic protein 2 (BMP2), the most widely used FDA-approved osteoinductive growth factor, is a nonspecific growth factor that contributes to various growth and developmental processes in the body. This functional heterogeneity of BMP2 is known to contribute to clinical complications such as ectopic bone formation[13] and promotion of adipogenesis, leading to cystic bone voids[14–16] that compromise the quality of regenerated bone. Moreover, increased complications have been reported with use of BMP2 in patients with osteoporosis, leading experts to suggest avoidance of its use in those with osteoporotic bone disease.[9]

Nel-like molecule-1 (NELL-1), a novel osteoinductive growth factor originally identified in patients with craniosynostosis, has previously been shown to be effective in bone regeneration in various *in vitro* and *in vivo* studies.[17–20] It has been shown to be osteoblast specific, and importantly, is able to suppress the side effects of cystic bone formation seen in high-dose usage of BMP2.[16] In our preliminary *in vivo* study using an ovariectomy (OVX)-induced osteoporotic mouse model, NELL-1 also demonstrated successful regeneration of bone when locally injected into femurs of 6-month-old mice (data not shown). These findings suggest a role for NELL-1 for bone regeneration in osteoporotic conditions. [Note: *NELL-1* and NELL-1 indicate the human gene and protein, respectively; *Nell-1* and Nell-1 indicate the animal gene and protein, respectively.]

In this study, we aim to demonstrate the capacity of NELL-1 to prevent OVX-induced osteoporosis in a senile rat model. We hypothesize that NELL-1, when injected locally into the bone marrow space of rat femurs, would effectively potentiate the osteogenic capacity of endogenous BMSCs and endosteal osteoblasts to prevent bone loss.

Materials and Methods

Experimental groups

Twenty-four 10-month-old female Sprague-Dawley rats (Charles River Laboratories) were used. Ten-month-old animals were used, as studies have shown that rats of this strain reach peak bone mass by 9 months; therefore, little-to-no bone modeling occurs that would confound our findings.[21] Animals were randomly assigned to the following groups:

- SHAM group as the nonosteoporotic control group. A total of six femurs were obtained from three animals, and were harvested at 8 weeks postsham operation. No animals underwent injection.
- OVX group as the osteoporotic control group. A total of six femurs were obtained from three animals, and were harvested at 8 weeks post-OVX operation. No animals underwent injection.
- NELL-1 groups were euthanized at 2, 4, and 8 weeks post-OVX and injection procedures. For each timepoint, one femur was injected with tricalcium phosphate (TCP) mixed with phosphate-buffered saline (OVX + PBS/TCP; control), and the contralateral femur was injected with NELL-1 lyophilized to TCP and mixed with PBS (OVX + NELL-1/TCP). A total of six control-treated femurs and six NELL-1-treated femurs were obtained from six animals for each timepoint.

Whole femurs were harvested for high-resolution microcomputed tomography (microCT), histology, and immunohistochemistry analyses after euthanasia. Rat uteri were also harvested and weighed wet and dry as confirmation of OVX as previously described.[22,23]

Injectate preparation

β-TCP of 10–50-μm particle size was used as a carrier to deliver and allow sustained release of NELL-1 as previously described.[24] The injectates consisted of 50 μL for each femur of 100 mg/mL β-TCP with or without 600 μg/mL of recombinant human (rh) NELL-1. The optimal dose of NELL-1 was determined based on our previous intramedullary injection study on healthy rat models (manuscript in preparation).

Surgical procedure

Animals were housed in a light- and temperature-controlled environment and given food and water *ad libitum*. All animals were handled in accordance with guidelines of the UCLA Chancellor's Animal Research Committee of the Office for Protection of Research Subjects.

Ovariectomy. Sprague-Dawley rats were anesthetized by isoflurane inhalation, and buprenorphine injection was administered before surgical incision. For OVX, a 5-mm dorsal incision was made on the flank of each rat between the bottom of the rib cage and the front of the hind limb. The tip of a double-sharp iridectomy scissors was inserted through the muscle layer, and the muscle fibers were separated. The ovary was pulled through the incision with a pair of blunt forceps by grasping the fat pad surrounding it. High-temperature surgical cautery (Bovie Medical) was used to resect the ovary and oviduct, and the fat pad was replaced into the body cavity after confirming hemostasis. The skin

incision was closed using 4-0 vicryl sutures. The procedure was repeated on the contralateral side.

For sham surgery, the fat pad was pulled through the incision with a blunt forceps following the same steps as above. The fat pad was replaced into the body cavity without resection of the ovary and oviduct. The skin incision was closed using 4-0 vicryl sutures. The procedure was repeated on the contralateral side.

Intramedullary injection. Knee arthrotomy and intramedullary injection of the femur were performed immediately after OVX. Briefly, a 5-mm-longitudinal incision was made along the medial aspect of the quadriceps–patellar complex. The patella was dislocated laterally to expose the intercondylar groove. A 0.9-mm k-wire on a trephine drill was used to create a trephination defect. A 26-gauge needle was inserted through the defect, and 50 μL of NELL-1/TCP injectate was injected into the intramedullary cavity. The trephination was sealed with bone wax after injection. The quadriceps–patellar complex was then repositioned, and the medial arthrotomy was carefully repaired with 5-0 vicryl sutures. About 50 μL of PBS/TCP as control was injected into the contralateral femur, following the same surgical procedure as above.

Radiographic evaluation

Posteroanterior radiographs were taken preoperation and at harvest using a high-resolution Faxitron LX-60 Cabinet radiography system at a resolution of 10 lp/mm.

Three-dimensional microCT evaluation

Postharvest, whole femurs were scanned using high-resolution microCT (Skyscan 1172; Skyscan) at an image resolution of 27.4 μm (50 kV and 201 mA radiation source, using a 0.5-mm aluminum filter), and analyzed using DataViewer, Recon, CTAn, and CTVol software provided by the manufacturer. The quantitative and structural parameters follow the nomenclatures described by the American Society for Bone and Mineral Research Nomenclature Committee.[25]

Femurs were analyzed in three separate regions—proximal femur (PF), mid-shaft (MS), and distal femur (DF)—to comply with published guidelines and to assess site-specific responses to OVX and treatment.[26,27] For analysis, well-established quantitative and structural microCT parameters, including bone mineral density (BMD), percent bone volume (BV/TV), trabecular number, thickness, and separation (Tb.N, Tb.Th, and Tb.S), were measured.

Femurs were first reoriented to an exact upright position in three planes of space (coronal, sagittal, and transaxial) using DataViewer software. Then, the highest point of the growth plate on the vertical axis was noted and used as the baseline level from which to divide the femurs into the three regions. Along the vertical axis, the secondary spongiosa at 1 mm proximal to the growth plate was set as the lower (distal) border of the DF to avoid inclusion of newly formed bone in the rats.[26] From this level, DF is designated as the lower 6.4 mm, MS as the middle 8.2 mm, and PF as the top 6.4 mm of the femur segment analyzed. These dimensions were determined by careful analysis of the anatomy of all femur samples and calculation of the average number of slices that could be universally applied to all samples.

In examining the scanned images of whole femurs to standardize the method of analysis, transaxial microCT images of the right and left femurs of each animal were generated at various levels along the vertical axis (Supplementary Fig. S1A; Supplementary Data are available online at www.liebertpub.com/tea). This was to determine the relative expansion or resorption of the periosteal and endosteal bone between the OVX+PBS/TCP control and OVX+NELL-1/TCP femurs, and also to examine the degree of variance between the right and left femurs of the SHAM and OVX groups. The newly formed bone was eliminated by differential thresholding for clearer assessment. The right femur in SHAM and OVX, as well as the OVX+NELL-1/TCP femurs at 2-, 4-, and 8-week groups were colored red, mirrored horizontally, and superimposed on the contralateral side in green using Adobe Photoshop CS4 (Supplementary Fig. S1B). This is similar to the previously published method of cortical bone analysis in the OVX rat model by Jee *et al.*, where the bones were analyzed in three distinct layers: inner, middle, and outer cortical zones.[26]

For analysis of trabecular bone, regions of interests (ROIs) were drawn to discreetly select trabecular bone only, maintaining ~0.25 mm clearance from the endosteal bone surface. For analysis of cortical bone, ROIs were drawn to fit exactly the outer border on the periosteal surface and the inner border on the endosteal surface.

To determine the optimal threshold, two representative femur pairs (based on radiographic findings) were selected from each group. The threshold for trabecular bone was set to 95–255 to match the normal bone structure in the SHAM and OVX+PBS/TCP control femurs and also partly include less-mature intramedullary bone. The threshold for cortical bone was set to 150–255 to match the normal bone structure in the SHAM and OVX+PBS/TCP control femurs while excluding the trabecular components, and was reassessed in other experimental groups. Three-dimensional images were generated to confirm that the optimized thresholds properly represent the bones. The selected thresholds were then applied to all samples in the experiment.

Histological and immunohistochemical analyses

After microCT analysis, the specimens were decalcified using Cal-Ex solution (Fisher Scientific) for 5 to 7 days, washed with running tap water for 3 to 4 h, and then transferred to 75% ethanol solution. The specimens were then processed for paraffin embedding, and 5-μm-sagittal sections of each specimen were obtained and stained with hematoxylin and eosin (H&E).

For immunohistochemistry, paraffin slices were deparaffinized, dehydrated, rinsed, and incubated with 3% H_2O_2 for 20 min and then blocked with 0.1% bovine serum albumin in PBS for 1 h. Primary antibodies, including anti-osteopontin (OPN) and anti-osteocalcin (OCN; Santa Cruz Biotechnology), at a dilution of 1:100 were added to each section and incubated at 37°C for 1 h and at 4°C overnight. ABC complex (Vector Laboratories) was applied to the sections after the incubation with biotinylated secondary antibody (Dako Corporation). AEC plus substrate in red color (Dako Corporation) was used as a chromagen, and the sections were counterstained with light hematoxylin. PBS substituted for the primary antibody was used as a negative

control. Photomicrographs were acquired using an Olympus BX51 microscope and a MicroFire digital microscope camera with PictureFrame software (Optronics).

Relative intramarrow adiposity was quantified using Adobe Photoshop. Relative lipid area was quantified using the Magic Wand tool, normalized to total marrow space within 20× magnification histological photomicrographs of the femurs.

In vitro *BMSC differentiation studies*

Primary rat bone marrow mesenchymal stem cells (BMSCs) were obtained from the femoral marrow cavity of Sprague-Dawley rats. BMSCs were obtained by marrow flush either 4 weeks after OVX or from age-matched controls. Passage-2 cells only were used for experiments. Cells were expanded in the Dulbecco's modified Eagle's medium at 37°C and 5% CO_2 as previously described.[28] For *in vitro* osteogenic differentiation, OVX and control BMSCs were seeded at equal densities (1.3×10^4 cells per cm^2). After attachment, the medium was replaced with an osteogenic differentiation medium (ODM). The medium was supplemented with either (rh)NELL-1 at 300 ng/mL[29–33] or control PBS. The ODM was replaced every third day. Cells were differentiated for 15 and 24 days for alkaline phosphatase (ALP) and alizarin red (AR) staining, respectively. Cells were fixed with 10% formalin for 10 min, and ALP staining (indicating intermediate osteogenic differentiation) and AR staining (indicating terminal osteogenic differentiation) were performed as previously described.[34] Photographic quantification was performed, assessing the relative intensity of staining by averaging 3 random microscopic fields using the Magic Wand Tool in Adobe Photoshop.

Statistical analysis

For statistical analysis, Student's *t*-test was performed paired to compare the PBS/TCP control and NELL-1/TCP femurs within the same treatment group ($^{*}p<0.05$ and $^{**}p<0.01$), and unpaired to compare two different groups ($^{\#}p<0.05$ and $^{\#\#}p<0.01$).

Results

Confirmation of rat OVX-induced osteoporosis model

Uteri were weighted 1 h (wet weight) and 12 h (dry weight) postharvest. There was a statistically significant decline in uterine weight of OVX samples versus SHAM, providing a surrogate marker for estrogen loss and osteoporosis induction (Supplementary Fig. S2).

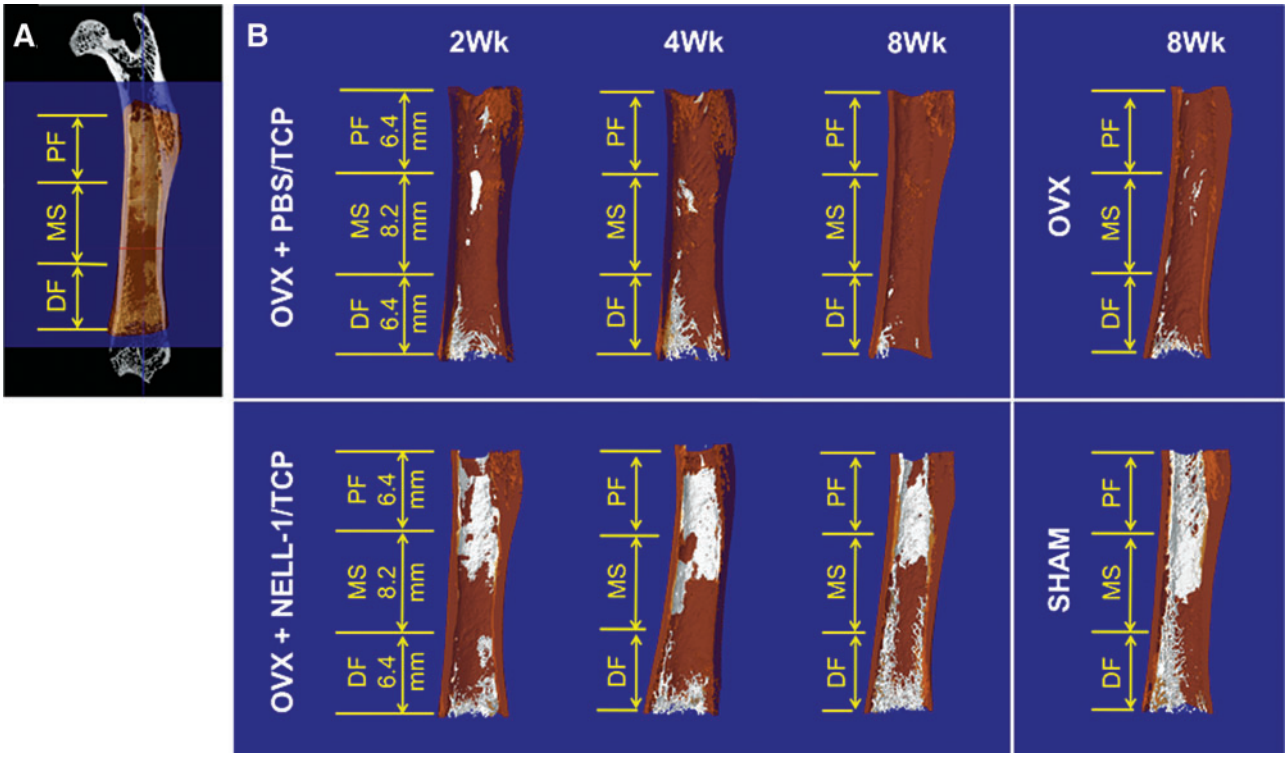

FIG. 1. Microcomputed tomography (microCT) three-dimensional (3D) reconstructions showing trabecular bone formation. Postharvest, whole femurs where analyzed using microCT. Cortical bone is represented in gray/black and trabecular bone in white in the 3D reconstruction. **(A)** Schematic of femur region designations, defining the proximal (PF), mid-shaft (MS), and distal femur (DF) as analyzed. **(B)** In the PF and MS regions, the ovariectomy (OVX) + phosphate-buffered saline (PBS)/tricalcium phosphate (TCP) control samples demonstrated continuous decrease in bone quantity and quality from 2 to 8 weeks, and approached the level of OVX only samples by 8 weeks. In contrast, the OVX + Nel-like molecule-1 (NELL-1)/TCP femurs maintained bone levels from 2 to 8 weeks, approaching SHAM levels by 8 weeks. The DF was least affected by either OVX or treatment, with minimal changes in trabecular bone. To visualize the inner trabecular bone, the cortical bone was hemisectioned coronally in 3D reconstructions. Color images available online at www.liebertpub.com/tea

Three-dimensional microCT

Trabecular bone. At 2-, 4-, and 8-week time-points, OVX + NELL-1/TCP femurs had significantly increased trabecular bone compared to OVX + PBS/TCP control femurs that showed progressive loss of bone in the PF and MS regions as shown by three-dimensional reconstructions in Figure 1. Quantitative analysis of femurs showed that BV/TV, BMD, and trabecular thickness and number of OVX + NELL-1/TCP femurs were comparable to that of the SHAM group and significantly increased when compared to the OVX + PBS/TCP control at 8 weeks in the PF and MS regions ($^{*}p < 0.05$, $^{**}p < 0.01$ compared to PBS/TCP control; $^{\#}p < 0.05$, $^{\#\#}p < 0.01$ compared to SHAM) as shown in Figures 2 and 3.

Overall, the DF region showed minimal effects of OVX-induced osteoporosis, and also showed the least difference between PBS/TCP and NELL-1/TCP sides. The OVX + NELL-1/TCP femurs, however, did show maintenance of bone over time, whereas OVX + PBS/TCP control femurs showed continuous loss of bone from 2, 4, and 8 weeks in the DF.

Cortical bone. Cortical bone did not show significant difference in BV/TV or BMD between groups (data not shown). This is in accordance with the literature that osteoporosis induced solely by OVX will not produce significant cortical changes in rats until after 6–9 months post-OVX.[35,36]

Histology and immunohistochemistry

H&E staining was performed on 2-, 4-, and 8-week treated femurs, and 8-week SHAM and OVX femurs. At 2 and 4 weeks, OVX + PBS/TCP and OVX + NELL-1/TCP samples showed similar levels of bone loss, mainly as thinning of trabecular structure (data not shown). By 8 weeks, OVX + PBS/TCP control femurs continued to show considerable reduction of lamellar bone, findings which were similar to that of the OVX group. Conversely, OVX + NELL-1/TCP femurs showed recovery of lamellar bone volume (BV), with very evident increase in endosteal-woven bone formation comparable to the SHAM group (Fig. 4A–H).

Immunohistochemistry showed significantly increased distribution and enhanced intensity of OPN (Fig. 4I–L) and OCN (Fig. 4M–P) immunostaining in the OVX + NELL-1/TCP-treated femurs than that of OVX + PBS/TCP- and OVX-alone controls. Moreover, the positive staining patterns of OPN and OCN appeared to be distinctly different; OPN was expressed predominantly along the active bone formation

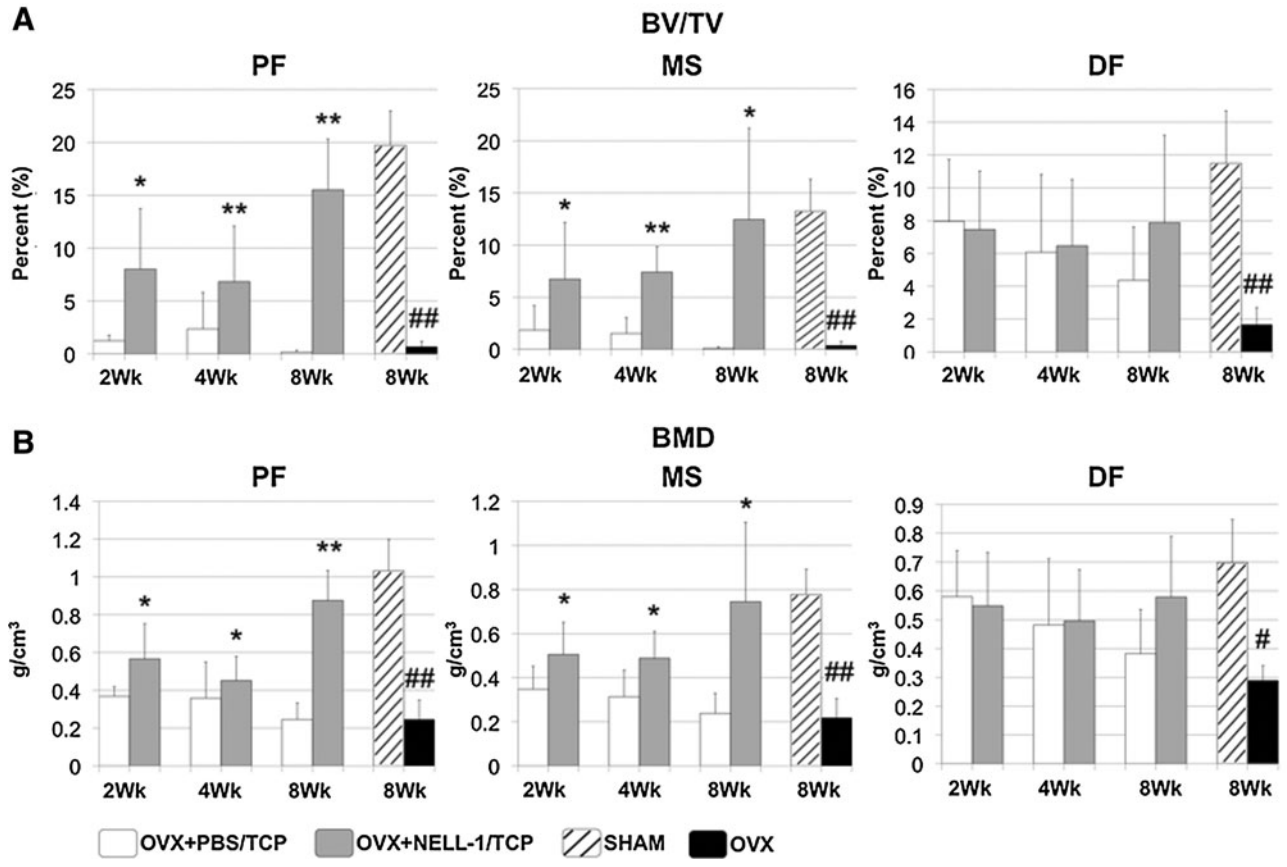

FIG. 2. Quantitative microCT analysis of trabecular bone volume (BV/TV) and bone mineral density (BMD). Trabecular bone was analyzed from the 2-, 4-, and 8-week OVX + NELL-1/TCP and OVX + PBS/TCP control-treated groups, as well as 8-week SHAM- and OVX-only groups in the PF, MS, and DF segments. **(A)** Analysis of percent bone volume (BV/TV) and **(B)** BMD. For both BV/TV and BMD, the difference between the SHAM- and OVX-only groups was statistically significant in PF and MS regions, but less in the DF region. Overall, the DF region was least affected by OVX and/or treatment. $^{*}p < 0.05$, $^{**}p < 0.01$ for paired *t*-test between the PBS/TCP and NELL-1/TCP groups within each time point; $^{\#}p < 0.05$, $^{\#\#}p < 0.01$ for one-way, unpaired *t*-test between the SHAM and OVX groups.

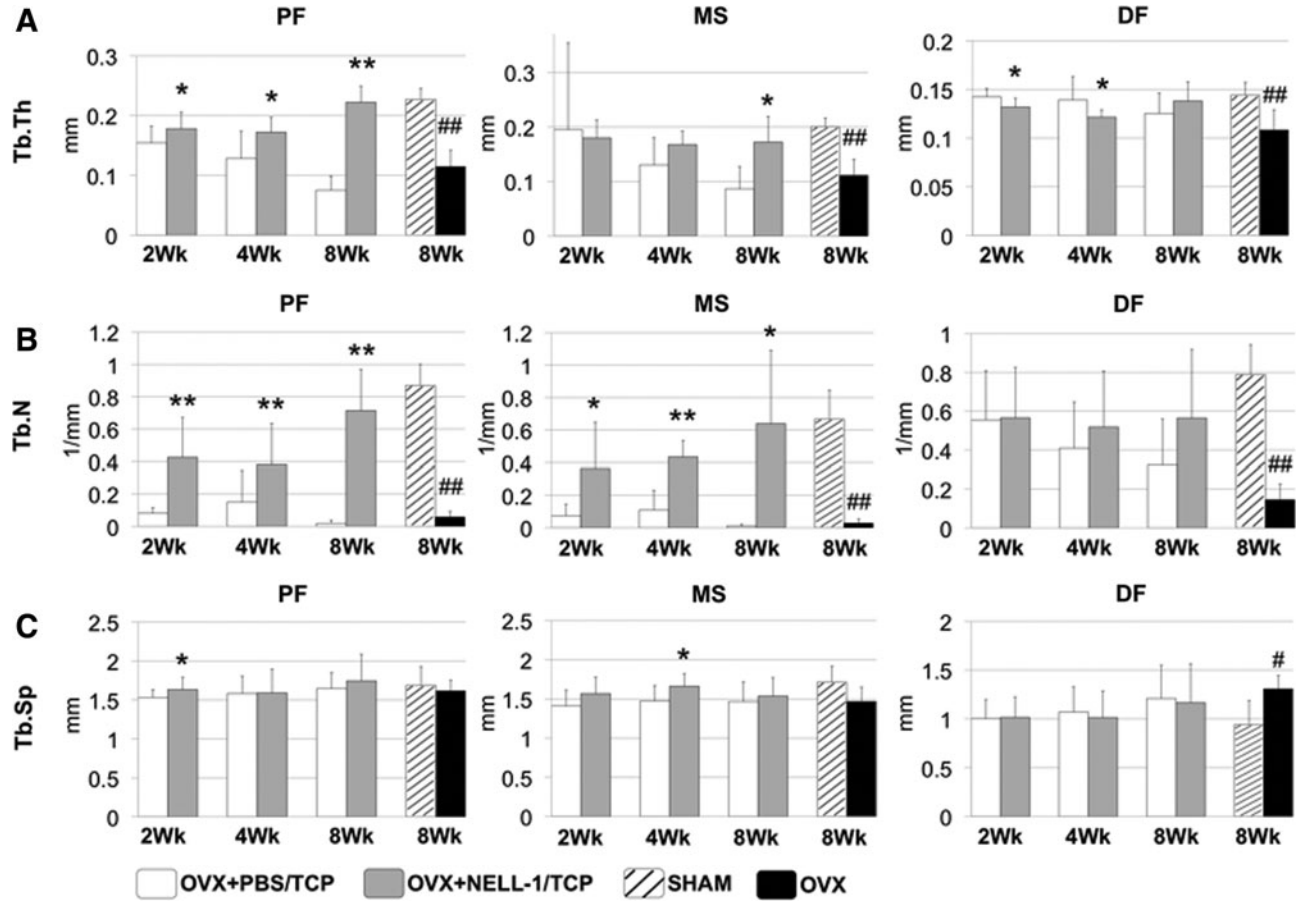

FIG. 3. Quantitative microCT analysis of trabecular space, thickness, and number. The structural parameters of trabecular bone were analyzed in the PF, MS, and DF regions. The OVX + PBS/TCP control femurs at 2, 4, and 8 weeks showed a decreasing trend in **(A)** trabecular thickness (Tb.Th) and **(B)** number (Tb.N), and an increase in **(C)** trabecular spacing (Tb.S) in all three PF, MS, and DF regions. OVX + NELL-1-/TCP-treated femurs showed an increasing trend in Tb.Th and Tb.N, reaching SHAM levels by 8 weeks. Statistically significant increases in Tb.Th and Tb.N were found between OVX + PBS/TCP control and OVX + NELL-1/TCP femurs in PF and MS, but less in DF. The trabecular parameters in DF region appeared to be the least affected by OVX and/or treatment. $^{*}p < 0.05$ and $^{**}p < 0.01$ for paired *t*-test between the PBS/TCP and NELL-1/TCP groups within each time point; $^{\#}p < 0.05$, $^{\#\#}p < 0.01$ for one-way, unpaired *t*-test between the SHAM and OVX groups.

fronts, while the OCN stains relatively mature bone matrix across all the samples. These results indicate that NELL-1 promotes more active woven bone formation and/or remodeling similar to that observed in SHAM control samples.

In addition, relative intramarrow adiposity quantification of histological images of OVX + PBS/TCP and OVX + NELL-1/TCP femurs at 8 weeks showed statistically significant reduction in lipid area, and thus adipogenesis in NELL-1-treated femurs (Fig. 5).

In vitro *results*

We next sought to confirm these results *in vitro*, examining the effect of (rh)NELL-1 delivered on BMSCs extracted from healthy (4 weeks post-SHAM) or ovariectomized (4 weeks post-OVX) rats. Osteogenic differentiation was performed and assessed by ALP staining to assess early differentiation (Fig. 6A–D), and AR staining to assess terminal differentiation (bone nodule formation, Fig. 6E–H). Quantification was performed by photographic assessment (Fig. 6I, J). At baseline, OVX was observed to result in a reduction in osteogenic differentiation by all markers. Among control BMSCs, NELL-1 increased osteogenic differentiation by both ALP and AR staining and quantification. This was also observed among OVX BMSCs, where NELL-1 increased all markers of osteodifferentiation. These findings were consistent with our preliminary data using adenoviral transduction of control LacZ or *Nell-1* (AdNell-1) to SHAM and OVX rat BMSCs (Supplementary Fig. S3).

Discussion

In this study, we demonstrated the ability of NELL-1 to prevent osteoporotic bone loss by local intramarrow injection. In the setting of OVX, NELL-1 injection maintained appendicular bone mass, as assessed by radiologic, histologic, and immunohistochemical methods.

Our osteoporotic model was carefully created to limit confounding factors that may affect the findings in this study. At 9 months or older, Sprague-Dawley rats have reached peak bone mass, and no longer undergoes periosteal expansion from growth at the long diaphyses, and any

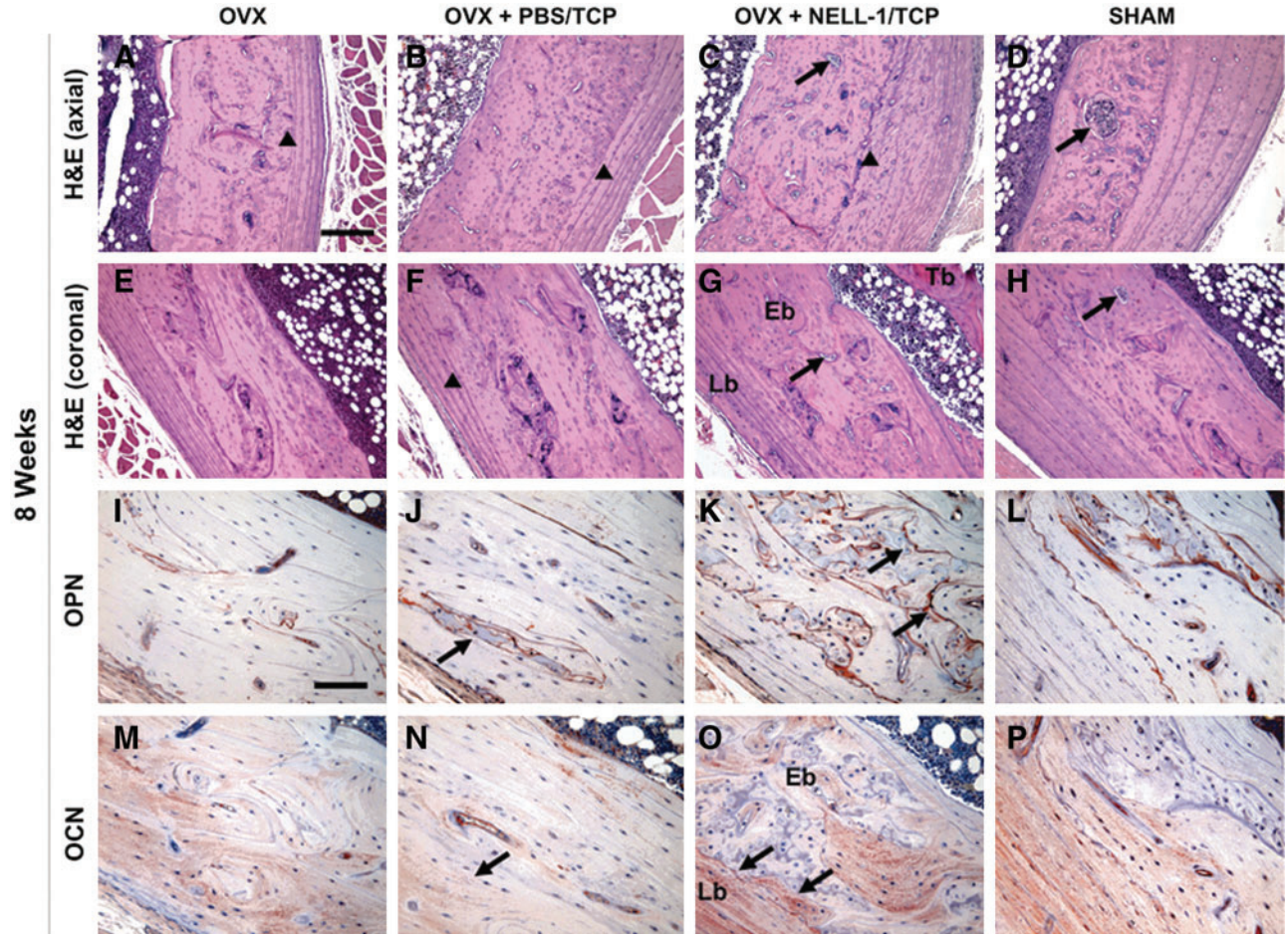

FIG. 4. Histologic assessment of bone formation. Representative hematoxylin and eosin (H&E) staining of transaxial mid-shaft **(A–D)**, and longitudinal sections **(E–H)** of femoral bones is shown from 8-week OVX + PBS/TCP control and OVX + NELL-1/TCP, and 8-week OVX-only and SHAM groups. Distinct differences in morphology between NELL-1 treatment and control is evident, with increased endosteal-woven bone encompassing small bone islands in OVX + NELL-1/TCP samples, indicating more active new bone formation (arrows). In addition, the thickness of the outer lamellar bone was increased in OVX + NELL-1/TCP samples (arrowheads), which is almost indistinguishable from that of SHAM control at 8 weeks. Scale bar: 200 μm for all H&E images. The distribution and intensity of osteopontin **(**OPN; **I–L)** and osteocalcin **(**OCN; **M–P)** immunostaining were significantly enhanced in OVX + NELL-1/TCP samples (arrows) indicating more active bone formation and remodeling compared to control-treated samples. Scale bar: 100 μm for all immunohistochemistry images. Lb, lamellar bone; Eb, endosteal bone; Tb, trabecular bone. Color images available online at www.liebertpub.com/tea

cortical remodeling will take place only on the inner cortical layer/endosteal surface of bone.[37,38] Of note, rats undergo menopause at 15 to 18 months of age.[39,40] Therefore, 10-month-old senile rats were used to undergo OVX to induce osteoporosis.

At the cellular level, osteoporosis is characterized by increased bone turnover rate, with an imbalance toward osteoclast-mediated bone resorption. NELL-1's capacity to reverse osteoporosis may be due to its modulation of osteoblast, osteoclast, and adipocyte activity. Mechanistically, *NELL-1* is a downstream mediator of Runt-related transcription factor 2 (Runx2), the key transcription factor regulating osteogenic differentiation. Runx2 regulates *NELL-1* expression by binding to its promoter region.[41] In turn, *NELL-1* upregulates Runx2 bioactivity by enhancing its phosphorylation through transient activation of mitogen-activated protein kinase signaling,[42] leading to promotion of bone formation. *NELL-1* overexpression has also been shown to partially rescue Runx2 haploinsufficiency.[43] In this study, we showed, *in vitro* and *in vivo*, NELL-1's capacity to promote osteogenesis.

With particular relevance to osteoporosis, multiple studies have found that BMSCs demonstrate defective or reduced osteogenesis.[44–46] Li *et al.* reported that BMSCs obtained from 3- and 6-month-old rats showed decreased proliferative and osteogenic potential compared to control BMSCs.[47] Our *in vitro* studies showed similar findings in which we showed reduced osteogenesis in OVX BMSCs as compared to control BMSCs. Although the exact mechanism of this decline is unknown, our studies showed that NELL-1 is able to reverse this effect. Addition of NELL-1 to OVX BMSCs leads to increased ALP and AR staining, to levels comparable to that of control BMSCs that received no NELL-1 treatment.

In vivo, NELL-1 protein is commonly delivered lyophilized onto TCP particles to increase its stability. Our previous publications have shown the release profile and confirmed

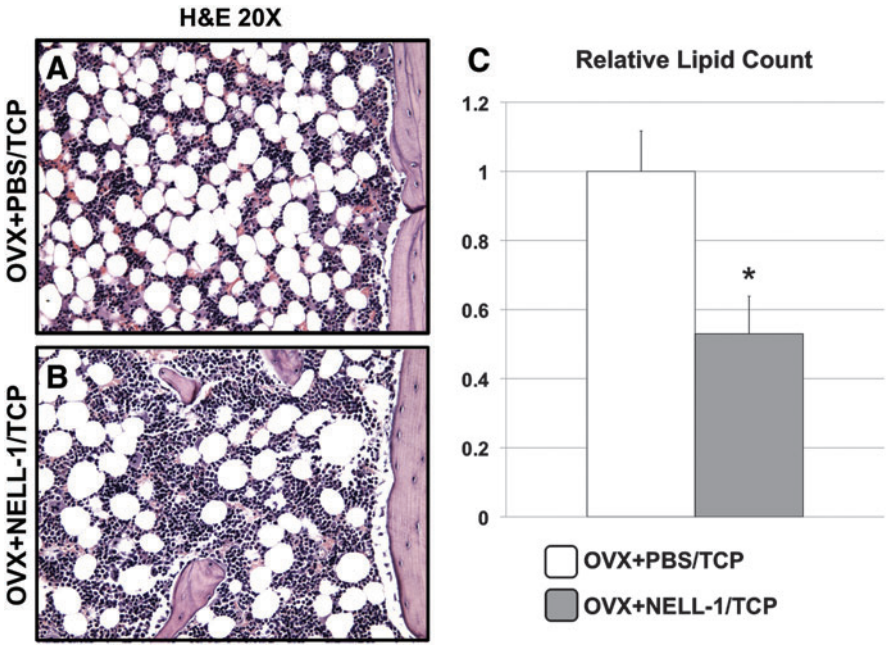

FIG. 5. H&E staining showing adipocyte count. Quantification of H&E histological images of **(A)** OVX + PBS/TCP and **(B)** OVX + NELL-1/TCP femurs at 8 weeks for relative intramarrow adiposity showed statistically significant reduction in lipid area with NELL-1 treatment **(C)**. $^{*}p < 0.05$. Color images available online at www.liebertpub.com/tea

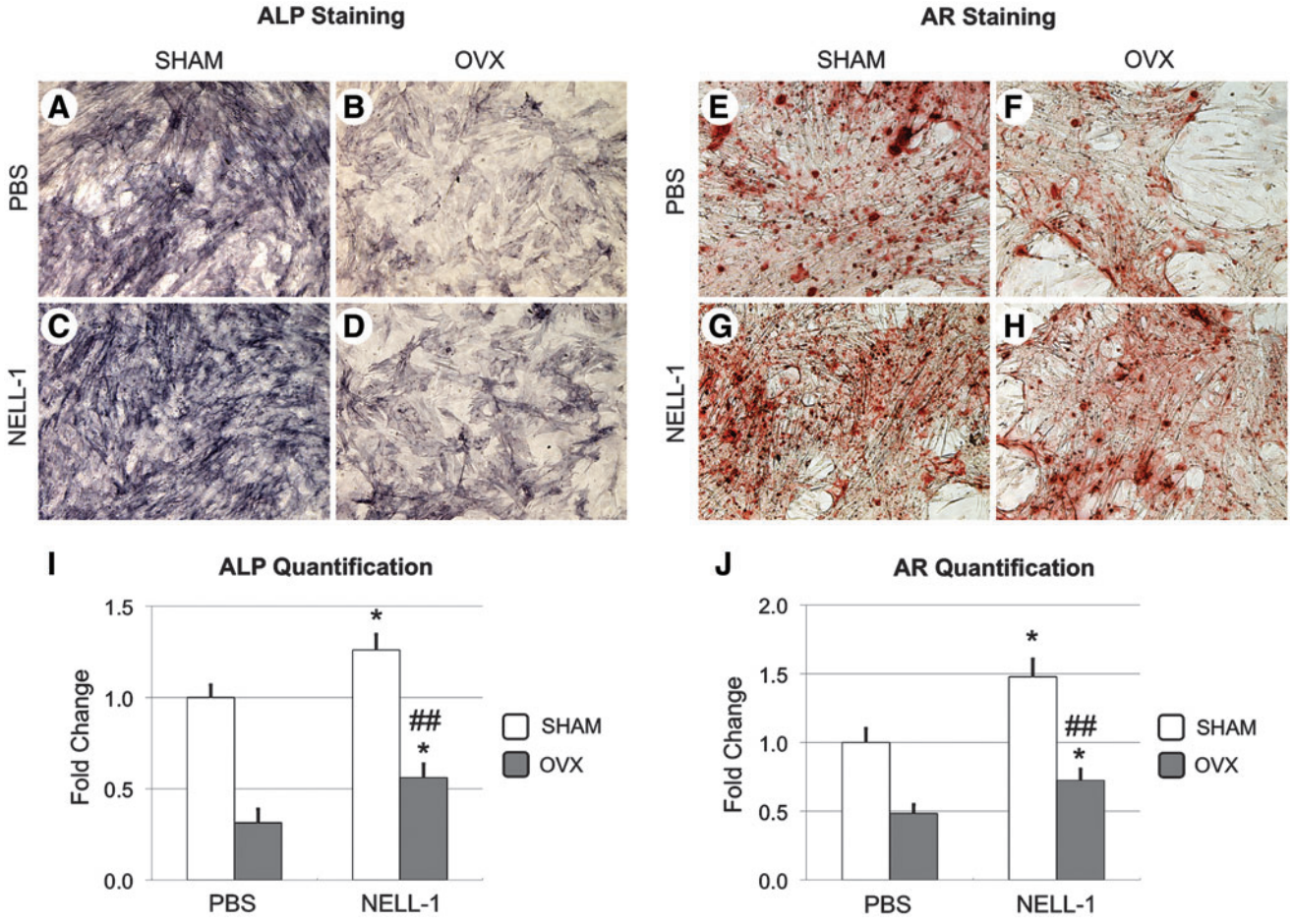

FIG. 6. *In vitro* osteogenic differentiation assays. The effects of NELL-1 on bone marrow stem cells (BMSCs) derived from SHAM or OVX rats were compared. **(A–D)** Assessment of early osteogenic differentiation by alkaline phosphatase (ALP) and **(E–H)** terminal differentiation/bone nodule formation by alizarin red (AR) staining showed reduction of all markers in the OVX BMSCs at baseline. Addition of NELL-1 increased osteogenic differentiation by both **(I)** ALP and **(J)** AR staining quantification in control and OVX BMSCs. $^{*}p < 0.05$ with respect to SHAM PBS, $^{\#\#}p < 0.01$ with respect to OVX PBS. Color images available online at www.liebertpub.com/tea

the *in vivo* bioactivities of the NELL-1/TCP delivery system.[48,49] In this study, we have found that although there was an initial decline in BV and BMD from 2 to 4 weeks post-OVX, NELL-1/TCP treatment resulted in an increase in bone levels similar to that of the SHAM control by 8 weeks. These findings were particularly significant in the proximal and mid-shaft regions of the femur. Overall, the DF showed less response to OVX as well as treatment and may be due to the proximity of the DF to the epiphyseal plate. Failure to show statistically significant differences of cortical bone between groups is not surprising, as previous studies have shown that osteoporosis induced solely by OVX will not produce significant cortical changes in rats until after 6–9 months post-OVX.[35,36]

Our previous studies have shown that NELL-1 stimulation of Runx2 may be through the canonical (β-catenin dependent) Wnt-signaling pathway, which is essential for differentiation of progenitor cells into osteoblasts.[50,51] While the mechanisms by which NELL-1 activates canonical Wnt signaling have not been determined, our previous *in vitro* studies showed that NELL-1 significantly induced β-catenin nuclear accumulation in M2-10B4 cells (JBMR manuscript in revision). We further confirmed NELL-1's association with Wnt signaling by performing studies co-applying NELL-1 with Wnt inhibitors. Addition of DICKKOPF-1 (DKK-1), a Wnt antagonist, eliminated NELL-1-induced increase in Runx2 expression in M2-10B4 cells (JBMR manuscript in revision).

NELL-1 has also been shown to downregulate peroxisome proliferator-activated receptor-gamma (PPAR-γ), a transcription factor and a master regulator of adipogenesis. This, again, may be mediated through NELL-1 effects on Wnt signaling, as Wnt signaling is known to inhibit PPAR-γ, and subsequently, adipogenesis in multiple cell lines.[52,53] Indeed, quantification of intramarrow adiposity of our histological results confirmed decreased adipocyte accumulation in the marrow of OVX+ NELL-1/TCP femurs compared to all other groups.

Finally, several lines of evidence suggest that loss of NELL-1 function is in fact associated with the development of bone loss and osteoporosis. We previously examined and reported on the skeletal phenotype of mice deficient in *NELL-1*. In the study, loss of *NELL-1* was produced by E-nitrosourea mutagenesis[54]; however, complete deficiency in *NELL-1* was shown to be neonatal lethal. After this finding, we have then examined adult and aged mice heterozyotes for *NELL-1* mutation induced the same way; preliminary results have demonstrated a clear osteopenic/osteoporotic phenotype that develops with age and is most prominent in the thoracic and lumbar spines. In ongoing studies, it appears that this is associated with reduced bone formation, and also inappropriately maintained bone resorption. Our newly discovered osteoporotic, *NELL-1*-deficient mouse model also has a human correlate. In a 2010 article, Karasik *et al.* evaluated over 430,000 single-nucleotide polymorphisms (SNPs) in over 2000 women in the Framingham Osteoporosis Study.[55] *NELL-1* was one of only 10 genes harboring an SNP found to be associated with reduced BMD in the femoral neck and lumbar spine. In aggregate, these observations span both animal research and clinical studies and suggest that the loss of NELL-1 function may in fact contribute to the natural development of osteoporosis.

In the context of the present study, these data suggest that NELL-1 may be not only a causative factor, but also a future therapeutic for osteoporotic bone loss. From this and previous studies, we know that NELL-1 increases local bone formation by increasing osteoblast differentiation and activity, but without a concomitant osteoclast response. These qualities make NELL-1 an appealing future therapy used for local application of NELL-1 in the prevention of fragility fractures in high fracture-risk patients. Further studies using higher mammals such as sheep that have similar cortical bone structure as humans, including the Haversian structures, are needed to evaluate NELL-1's effects on not only the trabecular, but also the cortical bone.

Conclusion

We demonstrated the ability of NELL-1 to successfully prevent the loss of BV, BMD, and trabecular microstructure in an OVX-induced osteoporotic senile rat model. Our *in vitro* and *in vivo* findings suggest NELL-1's capacity to harness and further enhance the osteogenic potential of endogenous BMSCs and endosteal osteoblasts in both healthy and osteoporotic bones.

Acknowledgments

The authors would like to thank the Translational Pathology Core Laboratory (TPCL) and Surgical Pathology divisions of the UCLA Department of Pathology and Laboratory Medicine for technical assistance with histology. This work was supported by the NIH/NIDCR (grants R21 DE0177711-01, DE01607-01, and R01 DE16107-05S1, ARRA Supplement), an UC Discovery Grant Bio07-10677, a T32 training fellowship (5T32DE007296-14) for Dr. A.W. James, and a CIRM Training Grant TG2-01169 for Dr. J. N. Zara.

Disclosure Statement

Drs. X.Z, K.T, and C.S. are inventors of NELL-1-related patents. Drs. X.Z, K.T, and C.S are founders of Bone Biologics, Inc., which sublicenses NELL-1 patents from the UC Regents.

References

1. National Osteoporosis Foundation. Clinician's Guide to Prevention and Treatment of Osteoporosis. Washington, DC, 2010.
2. U.S. Department of Health and Human Services. Bone Health and Osteoporosis: A Report of the Surgeon General. Rockville, MD: U.S. Department of Health and Human Services, Office of the Surgeon General, 2004.
3. Burge, R., Dawson-Hughes, B., Solomon, D.H., Wong, J.B., King, A., and Tosteson, A. Incidence and economic burden of osteoporotic fractures in the United States, 2005–2025. J Bone Miner Res **22,** 465, 2007.
4. Post, T.M., Cremers, S.C., Kerbusch, T., and Danhof, M. Bone physiology, disease and treatment: towards disease system analysis in osteoporosis. Clin Pharmacokinet **49,** 89, 2010.
5. Dominguez, L.J., Di Bella, G., Belvedere, M., and Barbagallo, M. Physiology of the aging bone and mechanisms of action of bisphosphonates. Biogerontology **12,** 397, 2011.
6. Kahn, A., Gibbons, R., Perkins, S., and Gazit, D. Age-related bone loss. A hypothesis and initial assessment in mice. Clin Orthop Relat Res **313,** 69, 1995.
7. Muschler, G.F., Nitto, H., Boehm, C.A., and Easley, K.A. Age- and gender-related changes in the cellularity of human

bone marrow and the prevalence of osteoblastic progenitors. J Orthop Res **19,** 117, 2001.
8. Gimble, J.M., Zvonic, S., Floyd, Z.E., Kassem, M., and Nuttall, M.E. Playing with bone and fat. J Cell Biochem **98,** 251, 2006.
9. Khan, S.N., and Lane, J.M. The use of recombinant human bone morphogenetic protein-2 (rhBMP-2) in orthopaedic applications. Expert Opin Biol Ther **4,** 741, 2004.
10. Vahle, J.L., Sato, M., Long, G.G., Young, J.K., Francis, P.C., Engelhardt, J.A., *et al.* Skeletal changes in rats given daily subcutaneous injections of recombinant human parathyroid hormone (1–34) for 2 years and relevance to human safety. Toxicol Pathol **30,** 312, 2002.
11. Tashjian, A.H., Jr., and Gagel, R.F. Teriparatide [human PTH(1–34)]: 2.5 years of experience on the use and safety of the drug for the treatment of osteoporosis. J Bone Miner Res **21,** 354, 2006.
12. Sewerynek, E., and Stuss, M. Bisphosphonates and the risk of atrial fibrillation. Endokrynol Pol **62,** 93, 2011.
13. Boraiah, S., Paul, O., Hawkes, D., Wickham, M., and Lorich, D.G. Complications of recombinant human BMP-2 for treating complex tibial plateau fractures: a preliminary report. Clin Orthop Relat Res **467,** 3257, 2009.
14. Carragee, E.J., Hurwitz, E.L., and Weiner, B.K. A critical review of recombinant human bone morphogenetic protein-2 trials in spinal surgery: emerging safety concerns and lessons learned. Spine J **11,** 471, 2011.
15. Sciadini, M.F., and Johnson, K.D. Evaluation of recombinant human bone morphogenetic protein-2 as a bone-graft substitute in a canine segmental defect model. J Orthop Res **18,** 289, 2000.
16. Zara, J.N., Siu, R.K., Zhang, X., Shen, J., Ngo, R., Lee, M., *et al.* High doses of bone morphogenetic protein 2 induce structurally abnormal bone and inflammation *in vivo*. Tissue Eng Part A **17,** 1389, 2011.
17. Ting, K., Vastardis, H., Mulliken, J.B., Soo, C., Tieu, A., Do, H., *et al.* Human Nell-1 expressed in unilateral coronal synostosis. J Bone Miner Res **14,** 80, 1999.
18. Desai, J., Shannon, M.E., Johnson, M.D., Ruff, D.W., Hughes, L.A., Kerley, M.K., *et al.* Nell1-deficient mice have reduced expression of extracellular matrix proteins causing cranial and vertebral defects. Hum Mol Genet **15,** 1329, 2006.
19. Siu, R.K., Lu, S.S., Li, W., Whang, J., McNeill, G., Zhang, X., *et al.* Nell-1 protein promotes bone formation in a sheep spinal fusion model. Tissue Eng Part A **17,** 1123, 2011.
20. Zhang, X., Kuroda, S., Carpenter, D., Nishimura, I., Soo, C., Moats, R., *et al.* Craniosynostosis in transgenic mice overexpressing Nell-1. J Clin Invest **110,** 861, 2002.
21. Jee, W.S., and Yao, W. Animal models of bone diseases. Introduction. J Musculoskelet Neuronal Interact **1,** 183, 2001.
22. Heneweer, M., Houtman, R., Poortman, J., Groot, M., Maliepaard, C., and Peijnenburg, A. Estrogenic effects in the immature rat uterus after dietary exposure to ethinylestradiol and zearalenone using a systems biology approach. Toxicol Sci **99,** 303, 2007.
23. Papaconstantinou, A.D., Umbreit, T.H., Fisher, B.R., Goering, P.L., Lappas, N.T., and Brown, K.M. Bisphenol A-induced increase in uterine weight and alterations in uterine morphology in ovariectomized B6C3F1 mice: role of the estrogen receptor. Toxicol Sci **56,** 332, 2000.
24. Li, W., Lee, M., Whang, J., Siu, R.K., Zhang, X., Liu, C., *et al.* Delivery of lyophilized Nell-1 in a rat spinal fusion model. Tissue Eng Part A **16,** 2861, 2010.
25. Parfitt, A.M., Drezner, M.K., Glorieux, F.H., Kanis, J.A., Malluche, H., Meunier, P.J., *et al.* Bone histomorphometry: standardization of nomenclature, symbols, and units. Report of the ASBMR Histomorphometry Nomenclature Committee. J Bone Miner Res **2,** 595, 1987.
26. Jee, W.S., and Yao, W. Overview: animal models of osteopenia and osteoporosis. J Musculoskelet Neuronal Interact **1,** 193, 2001.
27. Thompson, D.D., Simmons, H.A., Pirie, C.M., and Ke, H.Z. FDA Guidelines and animal models for osteoporosis. Bone **17,** 125S, 1995.
28. James, A.W., Leucht, P., Levi, B., Carre, A.L., Xu, Y., Helms, J.A., *et al.* Sonic Hedgehog influences the balance of osteogenesis and adipogenesis in mouse adipose-derived stromal cells. Tissue Eng Part A **16,** 2605, 2010.
29. James, A.W., Pang, S., Askarinam, A., Corselli, M., Zara, J.N., Goyal, R., *et al.* Additive effects of sonic hedgehog and nell-1 signaling in osteogenic versus adipogenic differentiation of human adipose-derived stromal cells. Stem Cells Dev **21,** 2170, 2012.
30. Zhang, X., Peault, B., Chen, W., Li, W., Corselli, M., James, A.W., *et al.* The Nell-1 growth factor stimulates bone formation by purified human perivascular cells. Tissue Eng Part A **17,** 2497, 2011.
31. Chen, F., Walder, B., James, A.W., Soofer, D.E., Soo, C., Ting, K., *et al.* NELL-1-dependent mineralisation of Saos-2 human osteosarcoma cells is mediated via c-Jun N-terminal kinase pathway activation. Int Orthop **36,** 2181, 2012.
32. Shen, J., Siu, R.K., Pang, S., Zara, J.N., Kwak, J., Zhang, X., *et al.* Novel Wnt regulator Nell-1 antagonizes BMP2-induced adipogenesis and augments BMP2-induced osteogenesis in rodent models. J Bone Miner Res 2012 (in Resubmission).
33. James, A.W., Askarinam, A., Zara, J.N., Corselli, M., Pan, A., Chang, L., *et al.* Human perivascular stem cells show enhanced osteogenesis and vasculogenesis with NELL-1 protein. Stem Cells Dev 2012 (in Resubmission).
34. Levi, B., James, A.W., Glotzbach, J.P., Wan, D.C., Commons, G.W., and Longaker, M.T. Depot-specific variation in the osteogenic and adipogenic potential of human adipose-derived stromal cells. Plast Reconstr Surg **126,** 822, 2010.
35. Ruth, E.B. Bone studies. II. An experimental study of the Haversian-type vascular channels. Am J Anat **93,** 429, 1953.
36. de Winter, F.R., and Steendijk, R. The effect of a low-calcium diet in lactating rats; observations on the rapid development and repair of osteoporosis. Calcif Tissue Res **17,** 303, 1975.
37. Li, X.J., Jee, W.S.S., Ke, H.Z., Mori, S., and Akamine, T. Age related changes of cancellous and cortical bone histomorphometry in female Sprague-Dawley rats. Cells Mater (Suppl) **1,** 25, 1992.
38. Schapira, D., Laton-Miller, R., Barzilai, D., and Silbermann, M. The rat as a model for studies of the aging skeleton. Cells Mater (Suppl) **1,** 181, 1992.
39. Steger, R.W., Huang, H.H., Chamberlain, D.S., and Meites, J. Changes in control of gonadotropin secretion in the transition period between regular cycles and constant estrus in aging female rats. Biol Reprod **22,** 595, 1980.
40. Miller, B.H., and Gore, A.C. N-Methyl-D-aspartate receptor subunit expression in GnRH neurons changes during reproductive senescence in the female rat. Endocrinology **143,** 3568, 2002.
41. Truong, T., Zhang, X., Pathmanathan, D., Soo, C., and Ting, K. Craniosynostosis-associated gene nell-1 is regulated by runx2. J Bone Miner Res **22,** 7, 2007.

42. Bokui, N., Otani, T., Igarashi, K., Kaku, J., Oda, M., Nagaoka, T., *et al.* Involvement of MAPK signaling molecules and Runx2 in the NELL1-induced osteoblastic differentiation. FEBS Lett **582,** 365, 2008.
43. Zhang, X., Ting, K., Bessette, C.M., Culiat, C.T., Sung, S.J., Lee, H., *et al.* Nell-1, a key functional mediator of Runx2, partially rescues calvarial defects in Runx2(+/-) mice. J Bone Miner Res **26,** 777, 2011.
44. Egermann, M., Heil, P., Tami, A., Ito, K., Janicki, P., Von Rechenberg, B., *et al.* Influence of defective bone marrow osteogenesis on fracture repair in an experimental model of senile osteoporosis. J Orthop Res **28,** 798, 2010.
45. Xiao, Y., Fu, H., Prasadam, I., Yang, Y.C., and Hollinger, J.O. Gene expression profiling of bone marrow stromal cells from juvenile, adult, aged and osteoporotic rats: with an emphasis on osteoporosis. Bone **40,** 700, 2007.
46. Chen, T.L. Inhibition of growth and differentiation of osteoprogenitors in mouse bone marrow stromal cell cultures by increased donor age and glucocorticoid treatment. Bone **35,** 83, 2004.
47. Li, D.J., Ge, D.X., Wu, W.C., Wu, J., and Li, L. [Osteogenic potential of bone marrow mesenchymal stem cells from ovariectomied osteoporotic rat]. Sichuan Da Xue Xue Bao Yi Xue Ban **36,** 318, 2005.
48. Lee, M., Li, W., Siu, R.K., Whang, J., Zhang, X., Soo, C., *et al.* Biomimetic apatite-coated alginate/chitosan microparticles as osteogenic protein carriers. Biomaterials **30,** 6094, 2009.
49. Lee, M., Siu, R.K., Ting, K., and Wu, B.M. Effect of Nell-1 delivery on chondrocyte proliferation and cartilaginous extracellular matrix deposition. Tissue Eng Part A **16,** 1791, 2010.
50. Gaur, T., Lengner, C.J., Hovhannisyan, H., Bhat, R.A., Bodine, P.V., Komm, B.S., *et al.* Canonical WNT signaling promotes osteogenesis by directly stimulating Runx2 gene expression. J Biol Chem **280,** 33132, 2005.
51. Brault, V., Moore, R., Kutsch, S., Ishibashi, M., Rowitch, D.H., McMahon, A.P., *et al.* Inactivation of the beta-catenin gene by Wnt1-Cre-mediated deletion results in dramatic brain malformation and failure of craniofacial development. Development **128,** 1253, 2001.
52. Ross, S.E., Hemati, N., Longo, K.A., Bennett, C.N., Lucas, P.C., Erickson, R.L., *et al.* Inhibition of adipogenesis by Wnt signaling. Science **289,** 950, 2000.
53. Zhou, S., Eid, K., and Glowacki, J. Cooperation between TGF-beta and Wnt pathways during chondrocyte and adipocyte differentiation of human marrow stromal cells. J Bone Miner Res **19,** 463, 2004.
54. Zhang, X., Ting, K., Pathmanathan, D., Ko, T., Chen, W., Chen, F., *et al.* Calvarial cleidocraniodysplasia-like defects with ENU-induced Nell-1 deficiency. J Craniofac Surg **23,** 61, 2012.
55. Karasik, D., Hsu, Y.H., Zhou, Y., Cupples, L.A., Kiel, D.P., and Demissie, S. Genome-wide pleiotropy of osteoporosis-related phenotypes: the Framingham Study. J Bone Miner Res **25,** 1555, 2010.

Address correspondence to:
Chia Soo, MD
Department of Orthopaedic Surgery
University of California, Los Angeles
Los Angeles, CA 90095-1579

E-mail: bsoo@ucla.edu

Received: January 26, 2012
Accepted: August 24, 2012
Online Publication Date: December 10, 2012